PHYSICAL REVIEW B VOLUME 24, NUMBER 12 15 DECEMBER 1981

Pressure dependence of the relativistic band edges of trigonal Te and Se

J. von Boehm and H. M. Isomäki
Electron Physics Laboratory and Department of General Sciences,
Helsinki University of Technology,
SF-02150 Espoo 15, Finland
(Received 1 June 1981)

The pressure dependence of the valence- and conduction-band edges of trigonal Te and Se is studied theoretically by a self-consistent relativistic *ab initio* level calculation. The agreement with the experimental $\vec{k}\cdot\vec{p}$ models is close for Te at 0 kbar. The differences are associated with the missing mass-velocity term in the $\vec{k}\cdot\vec{p}$ theory. The double valence-band maximum of Se near point M shifts at ~ 35 kbar to the vicinity of point H where it attains the two-ellipsoidal→dumbbell shape. After ~ 35 kbar the valence-band edge of Se behaves qualitatively similarly to that of Te (the double maximum tends to change into a single one). Large anisotropic changes induced by pressure are found, especially in the conduction-band edge of Se.

I. INTRODUCTION

Trigonal Te and Se, both being group-VI semiconductors, have an uncommon anisotropic crystal structure consisting of helical chains arranged in a hexagonal lattice. The main effect of the application of hydrostatic pressure P is to bring the chains closer. This causes the rich and often unexpected physical behavior of these materials under pressure. The anomalous behavior of the optical spectra of Se under pressure has been interpreted either with[1,2] or without[3,4] local-field corrections. The behavior of trigonal Te and Se under high pressures, as a part of the complex phase diagram, has also been recently subject to active study.[5–13] The key quantities for the understanding of the above and other pressure-dependent phenomena of these materials are the relativistic valence bands (VB) and conduction bands (CB) and especially their edges.

It is quite generally accepted that the VB maxima of Te at $P=0$ kbar are characterized by two-ellipsoidal→dumbbell-shaped constant-energy surfaces near the corner points H (or H') of the first Brillouin zone (BZ).[14] An interesting feature is the tendency of these double maxima to transform into single ones under pressure[15] which has been observed by Shubnikov–de Haas,[16] transport,[17,18] and optical[18,19] experiments. The conclusions drawn from these experiments are based on the parametrized $\vec{k}\cdot\vec{p}$ perturbation theory, which also includes the spin-orbit coupling. One of the aims of this work is to study whether a relativistic self-consistent *ab initio* level calculation can give the same behavior for the VB edge. A discussion of the effects of the Darwin and mass-velocity terms on the results is given. We also present results for the P dependence of the CB edge of Te.

The P-dependent behavior of the band edges of the more anisotropic Se can be expected to be even richer than that of Te. Because of the higher anisotropy the double VB maxima of Se are located near the center points M of the HMH' axes of BZ at $P=0$ kbar.[9,10,20] Under applied hydrostatic pressure Se becomes more isotropic and the VB maxima shift at $P\approx 35$ kbar from the neighborhood of the points M to the vicinity of points H.[8,9,21] It is then interesting to compare the behavior of the VB (and also CB) edges of isostructural Se and Te under pressure.

All the self-consistent calculations used thus far for the pressure-dependent behavior of Te and Se have been nonrelativistic.[4,7–11,22] However, the inclusion of the relativistic effects is crucial for the proper description of the VB or CB edges.[23,24] In this work we are going to report such a relativistic pressure-dependent study for Te and Se (the first to our knowledge). It is hoped that this work will stimulate experimental studies especially on the pressure dependence of the VB edge of Se.

The format of this paper is as follows. In Sec. II we present the methods. Section III contains the results and discussion and Sec. IV conclusions.

II. METHODS

Our calculations are of an *ab initio* type in the sense that the only parameters entering the calculations are the lattice constants listed in Table I (Refs. 25–29) and Slater's exchange-correlation constant.[30] As the starting point for the present calculation we use the general (non-muffin-tin) potentials resulting from the nonrelativistic self-consistent band calculations described in Refs. 10 and 11. First the nonrelativistic bands and wave functions near the band extrema are calculated with the self-consistent potential and with the basis of 235 orthogonalized plane waves. Then the relativistic bands are calculated with the degenerate first-order perturbation theory using the relativistic part of the Foldy-Wouthuysen Hamiltonian

$$H'=-i\frac{\alpha^2}{4}\vec{\sigma}\cdot(\nabla V)\times\nabla+\frac{\alpha^2}{8}(\nabla^2 V)-\frac{\alpha^2}{8}\nabla^4 \quad (1)$$

as the perturbation operator (given in the Hartree atomic units). α is the fine-structure constant, $\vec{\sigma}$ the Pauli spin operator, and V the crystal potential.

The earlier relativistic calculations with the orthogonalized plane-wave basis[31–34] used a non-self-consistent potential. However, to our knowledge the fundamental equations for the self-consistent case have not appeared in literature and are given in the Appendix. Some aspects of the computation are also discussed there.

III. RESULTS AND DISCUSSION

The VB maximum of Te is located at the corner point H under hydrostatic pressures up to ~40 kbar.[8,11] The behavior of the calculated uppermost and next-uppermost relativistic VB (solid lines) under pressure together with the corresponding experimental $\vec{k}\cdot\vec{p}$ model[19] (dashed lines) are shown in Figs. 1 and 2, respectively. In agreement with the $\vec{k}\cdot\vec{p}$ model the calculated VB maximum is of double type with the associated two-ellipsoidal →dumbbell-shaped constant-energy surfaces [Figs. 1(a) and 1(b)]. The calculated VB maximum also shows a tendency to change into a single maximum under pressure [Figs. 1(b) and 1(d)].

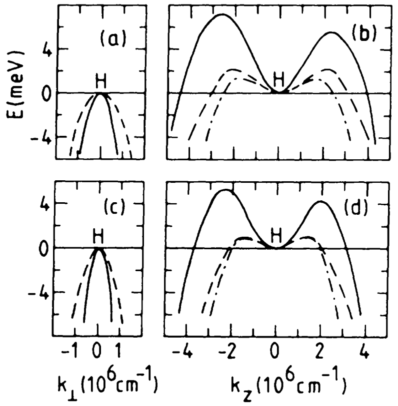

FIG. 1. Pressure dependence of the relativistic valence-band edge of Te. Solid lines represent the fully relativistically corrected bands, dash-dotted lines the spin-orbit-corrected ones, and dashed lines the $\vec{k}\cdot\vec{p}$ result (see Ref. 19). Pressures: (a) and (b) $P=0$ kbar, (c) and (d) $P=8$ kbar. In drawing the dash-dotted curve a small asymmetry in top heights was averaged away. $\vec{k}_H=\frac{1}{3}(\vec{b}_1+\vec{b}_2)+\frac{1}{2}\vec{b}_3$ is used as the origin ($\vec{b}$ denotes reciprocal-lattice vectors).

The accuracy of the calculated line shape may be estimated from the difference of the heights of the symmetrical tops on the k_z axis to be ~1 meV [see Fig. 1(b)]. This accuracy is an order of magnitude

TABLE I. Lattice constants.

Material	P (kbar)	a (nm)	c (nm)	u (a)
Te	0	0.44572[a]	0.5929[a]	0.2633[a]
	8	0.4378[b]	0.5948[b]	0.2670[c]
Se	0	0.4366[d]	0.4955[d]	0.2285[d]
	52	0.3878[d]	0.5139[d]	0.248[d]

[a] Reference 25.
[b] Reference 26.
[c] Reference 27.
[d] References 28 and 29.

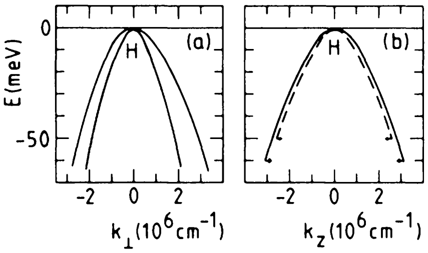

FIG. 2. Pressure dependence of the edge of the second-uppermost valence band of Te. Solid lines represent the fully relativistically corrected bands, dashed line the $\vec{k}\cdot\vec{p}$ result (see Ref. 19). In (a) the upper and lower curves are at 0 and 8 kbar, respectively. In (b) the change from 0 to 8 kbar is indicated by horizontal arrows.

better than what is usually considered to be a good accuracy in band calculations. The accuracy of ~1 meV may still be quite adequate in the small region of the $\vec{k}$ space near the band extrema, especially because only the band shape is considered. However, because the salient features of the band edges are of the order of a few meV the following comparison between the experimental and calculated results should be considered with slight reservations.

We find the following two main quantitative differences between the calculated VB maximum and the $\vec{k}\cdot\vec{p}$ models. Firstly, at $P=0$ kbar the hills (measured from the saddle point) on the k_z axis (height ~6 meV) are significantly higher than the $\vec{k}\cdot\vec{p}$ ones of 1.1–2.9 meV (Refs. 16, 19, and 35–38) [see also Fig. 1(b)]. Secondly, the $\vec{k}\cdot\vec{p}$ hills decrease more than twice as fast as the calculated ones under hydrostatic pressure from 0 to 8 kbar (Ref. 19) [cf. Figs. 1(b) and 1(d)].

The reason for the difference in the hill heights may be associated with the fact that the Darwin and mass-velocity terms [second and third term on the right-hand side of Eq. (1)] are neglected in the parametrized $\vec{k}\cdot\vec{p}$ theory. The Darwin term could be included in the $\vec{k}\cdot\vec{p}$ fitting scheme just by changing the meaning of the parameters, but the mass-velocity operator would introduce new terms proportional to $(\vec{k}\cdot\vec{p})^2$, $(\vec{k}\cdot\vec{p})\vec{p}^{\,2}$, and $\vec{p}^{\,4}$ which would, to some extent, change the structure of the $\vec{k}\cdot\vec{p}$ scheme. These terms are not negligible. A direct calculation with only the spin-orbit operator yields an uppermost VB (dash-dotted line in Fig. 1) which differs significantly from the fully corrected VB (solid line in Fig. 1) but agrees fairly well with the $\vec{k}\cdot\vec{p}$ fits[16,19,35–38] [see also Fig. (1b)]. However, the $\vec{k}\cdot\vec{p}$ hill still decreases almost twice as fast as the spin-orbit corrected one [cf. Figs. 1(b) and 1(d)]. Hence, this type of reasoning cannot fully explain the pressure dependence. Our result may possibly indicate that the fine structure in the experimental absorption spectrum does not directly reflect the pressure-dependent behavior of the VB edge. In fact only the lower (so-called α) peak at 126.3 meV is associated with a transition from the second-uppermost VB to the saddle point of the uppermost VB at H whereas the upper (so-called β) peak at 128.7 meV is associated with a transition

TABLE II. The effective hole masses of Te. $k_\perp$ and k_z denote the location from point H in units 10^6 cm^{-1}. Direction is given with respect to c axis. U and NU denote the uppermost and next-uppermost valence bands, respectively.

Band	P (kbar)	$k_\perp$	k_z	Direction	Theory[a]	Expt.
U	0	0	0	⊥	0.05	0.10[b]
		0	≈±2	‖	0.20	0.256[c]
		0	0	‖	−0.18	−0.29[d]
	8	0	0	⊥	0.02	
		0	≈±2	‖	0.14	
		0	0	‖	−0.23	
NU	0	0	0	⊥	0.05	0.26[d]
		0	0	‖	0.05	0.04[d]

[a] Present work

[b] Reference 40.

[c] Reference 41.

[d] Reference 38.

between the impurity levels near both band edges.[19] A disturbing factor here is that the α peak is observed also at low hole concentrations and low temperatures when the states near the saddle point should be occupied. Another related point is the fact that the β peak grows faster than the α one with increasing hole concentration.[39]

The calculated effective hole masses are compared with the experimental ones in Table II.[38,40,41] We find that the calculated values are smaller than the experimental values. This reflects again the fact that the experimental $\vec{k}\cdot\vec{p}$ bands are flatter than the calculated ones, possibly because of the missing mass-velocity (and Darwin) term.

The pressure dependence of the effective masses can also be obtained directly from conductivity measurements. Koma *et al.*[17] find that the (hole) mobility of the perpendicular sample at $P=7$ kbar reaches 2.15 times the one at $P=0$ kbar, whereas that of the parallel sample becomes only 1.78 times the one at $P=0$ kbar. We find for the corresponding ratios ~ 2.5 (obtained at the saddle point) and ~ 1.5 (P increased from 0 to 8 kbar). This agrees quite closely with the experiment.

The pressure dependence of the calculated next-uppermost VB [the change from 0 to 8 kbar indicated by arrows in Fig. 2(b)] is about the same as that of the experimental one.[19] We also notice that the changes induced by pressure are much larger in the $k_\perp$ direction [Fig. 2(a)] than in the k_z direction [Fig. 2(b)]. This is due to the fact that the main effect of the hydrostatic pressure is to bring the chains closer increasing the interchain interaction.

The calculated relativistic splittings of the VB of Te at point H, caused by the spin-orbit term, are presented in Table III (Refs. 19, 38, and 39) (the H_4 band is here assumed to be uppermost). The calculated differences are slightly smaller than the experimental ones. This is probably due to the locality of Slater's exchange-correlation potential which is known to result in energy spectra which are too compressed. Nevertheless, the calculated increase of the H_4-H_5 splitting under pressure from 0 to 8 kbar of 0.01 eV is in good agreement with the experimental value of 0.011 eV (Table III).

The (non-self-consistent) Korringa-Kohn-Rostoker (KKR) calculation gave 0.13 eV for the H_4-H_5 splitting[42] in close agreement with the experimental value. The H_5-H_6 distance from this calculation is only ~ 0.015 eV—an order of magnitude smaller than the H_4-H_5 one. This coincidence of the H_5 and H_6 band edges at almost the same energy has been used in interpreting optical-absorption spectra.[43,44] However, our calculated H_5-H_6 separation of 0.33 eV (Table III) as well as the experimental estimate of 0.48 eV (Ref. 38) are significantly larger than the KKR value.

The uppermost relativistically corrected VB of Se at $P=0$ kbar on the $H'MH$ axis is shown in Fig. 3. VB at point M (where the relativistic band is degenerate because of time-reversal symmetry) is ~ 0.19 eV higher than VB at point H (Table III).

TABLE III. The relativistic splitting of the uppermost valence band of trigonal Te and Se. The energy differences are given in eV. The H_4 band is assumed to be uppermost.

Material	P (kbar)	Difference	Theory[a]	Expt.
Te	0	H_4-H_5	0.09	0.126[b]
		H_5-H_6	0.33	0.48[c]
	8	H_4-H_5	0.10	0.137[d]
		H_5-H_6	0.32	
Se	0	$M_{1,2}$-H_4	0.19	
		H_4-H_5	0.02	
		H_5-H_6	0.18	
	52	H_4-$M_{1,2}$	0.26	
		H_4-H_5	0.04	
		H_5-H_6	0.17	

[a] Present calculation.
[b] Reference 39.
[c] Reference 38.
[d] Reference 19.

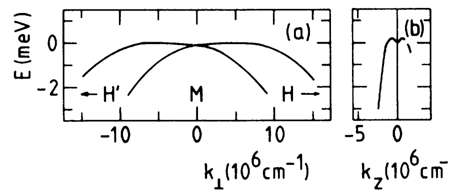

FIG. 3. Relativistic valence-band edge of Se at $P=0$ kbar. A slight asymmetry caused by numerical inaccuracies has been corrected in drawing the curves. $\vec{k}_M=\frac{1}{2}\vec{b}_1+\frac{1}{2}\vec{b}_3$ is used as the origin.

We find two symmetrically spaced VB maxima on the $H'MH$ axis near point M [Fig. 3(a)]. However, in the $k_\perp k_z$ plane these maxima represent only the maxima of a valley along the $H'MH$ axis. This is obvious from Fig. 3(b) where the uppermost VB is shown in the k_z direction at $k_\perp \approx 10^7$ cm^{-1}. One can expect a qualitatively similar behavior in all directions perpendicular to the MH axis. Therefore, the VB maxima inside BZ can be expected to be located pairwise at general points near the $H'MH$ axes at the angles of 120° around the ΓA axis. The calculated VB edge differs from the band model suggested by Moreth[20] as follows. Firstly, the calculated distance of the VB maxima from point M is $\sim 6\times 10^6$ cm^{-1} [Fig. 2(a)] which is about one third of the value of $\sim 17\times 10^6$ cm^{-1} proposed by Moreth.[20] Secondly, the calculated VB maxima lie at general points whereas in the model suggested by Moreth they are located on the HMH' axes. (Thirdly, as will be discussed below, the calculated CB minima are nondegenerate and lie on the HK axes whereas in the model proposed by Moreth the CB minima are degenerate and lie at point H.)

Figure 4 shows that the uppermost VB of Se at point H has transformed under pressure from a (local) minimum at $P=0$ kbar (dashed line) into a two-ellipsoidal→dumbell-shaped maximum at $P=52$ kbar (solid line). The uppermost VB at point M is ~ 0.26 eV lower than at point H at $P=52$ kbar (Table III). Especially noteworthy is the strong bending down of the uppermost VB on the $k_\perp$ axis [Fig. 4(a)] caused by the significant increase in the interchain coupling (Table I). The VB maximum hills of Se at $P=52$ kbar are more extended in the $\vec{k}$ space (maxima at $k_z \approx \pm 5\cdot 10^6$ cm^{-1}) and higher (height ~ 21 meV) than those of Te at $P=0$ kbar [Fig. 1(b)]. The hills diminish with increasing pressure qualitatively as in the case of Te [Fig. (4b)].

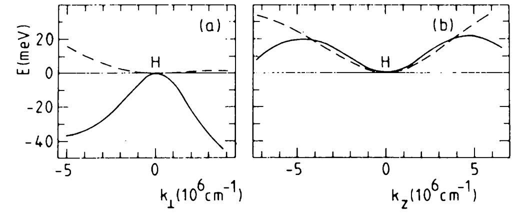

FIG. 4. Pressure dependence of the uppermost relativistic valence band of Se near point H. Dashed curves $P=0$ kbar, solid curves $P=52$ kbar. $\vec{k}_H=\frac{1}{3}(\vec{b}_1+\vec{b}_2)+\frac{1}{2}\vec{b}_3$ is used as the origin.

The spin-orbit splitting of VB at point H is smaller for Se than for Te (Table III) as can be expected from the corresponding atomic numbers 34 and 52. The main effect of the pressure is to move the H_5 band away from the H_4 band towards the H_6 band for both materials.

The CB minimum of both materials is located near point H. The calculated pressure dependence of CB near point H is shown in Figs. 5(a) and 5(b) for Te and Se, respectively. At $P=0$ kbar the $\vec{k}\cdot\vec{p}$ CB of Te based on the magnetoabsorption measurements[45] [dashed lines in Fig. 5(a)] and the calculated CB [solid lines in Fig. 5(a)] agree relatively closely on the k_z axis. The $\vec{k}\cdot\vec{p}$ bands are slightly flatter than the calculated bands which may again possibly be associated with the missing mass-velocity and Darwin terms in the $\vec{k}\cdot\vec{p}$ bands. The CB of Te change relatively little on the k_z axis when pressure is increased from 0 kbar [solid lines in Fig. 5(a)] to 8 kbar [dash-dotted lines in Fig. 5(a)] whereas the change on the $k_\perp$ axis is significantly larger because of the increased interchain interaction.

When pressure is increased from 0 to 52 kbar

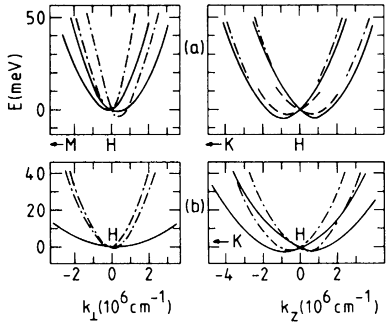

FIG. 5. Pressure dependence of the conduction-band edge of Te and Se. (a) Bands of Te, solid and dash-dotted lines represent the fully relativistically corrected bands at $P=0$ and 8 kbar, respectively, the dashed lines the $\vec{k}\cdot\vec{p}$ result at $P=0$ kbar (see Ref. 45). (b) Bands of Se, solid and dash-dotted lines represent the fully relativistically corrected bands at $P=0$ and 52 kbar, respectively. $\vec{k}_H=\frac{1}{3}(\vec{b}_1+\vec{b}_2)+\frac{1}{2}\vec{b}_3$ is used as the origin.

the changes in the CB of Se are much larger than in the case of Te. The effective mass of electrons along the k_z direction is decreased from ~ 0.13 to ~ 0.07 [Fig. 5(b)]. On the $k_\perp$ axis the changes are dramatic because of the strong increase of the interchain coupling (see Table I). Firstly for $k_\perp \approx \pm 2 \cdot 10^6$ cm^{-1}, the spin-orbit splitting which is < 1 meV at $P=0$ kbar grows to $\gtrsim 5$ meV at $P=52$ kbar. Secondly, the effective mass decreases from ~ 0.25 to ~ 0.05 [see Fig. 5(b)].

We finally comment on the difficult question of the size of the minimum optical gap between VB and CB. It is well known that self-consistent nonrelativistic band calculations with a local exchange-correlation potential tend to underestimate the gap. The relativistic corrections reduce the gap further. Our calculations confirm this situation. The nonrelativistic gaps of 0.24 (Ref. 11) and 0.92 eV (Ref. 10) for Te and Se, respectively, are smaller than the corresponding experimental values of 0.33 (Ref. 15) and 1.85 eV (Ref. 20). After the full relativistic corrections are included the gaps are reduced to -0.1 and 0.8 eV, respectively.

IV. CONCLUSIONS

We have presented the relativistic *ab initio* level calculations for the band edges of trigonal Te and Se. The calculated valence- and conduction-band edges for Te agree relatively closely with the experimental $\vec{k}\cdot\vec{p}$ models. However, the $\vec{k}\cdot\vec{p}$ bands are, in general, somewhat flatter than the calculated ones which may possibly be due to the neglect of the mass-velocity term in the $\vec{k}\cdot\vec{p}$ scheme. This view is supported by the fact that the uppermost valence band of Te calculated including only the spin-orbit term agrees much more closely with the $\vec{k}\cdot\vec{p}$ models than the fully corrected valence band does.

The $\vec{k}\cdot\vec{p}$ hills (based on the direct absorption measurement[19]) of the double valence-band maximum of Te diminish about twice as fast as the calculated ones. On the other hand, the pressure dependences of the effective masses of the conductivity measurement[17] and of our calculation agree quite closely. This may possibly indicate that the α-β fine structure in the absorption spectrum does not directly reflect the pressure-dependent behavior of the valence-band edge.

In the case of Se the double valence-band maxima near points M shift at ~ 35 kbar to the vicinity of points H (Refs. 9 and 21) and attain the two ellipsoidal→dumbbell shape. The behavior of the uppermost valence band of Se is, after this, qualitatively similar to that of Te.

Due to the anisotropy of Te and Se the behavior of the bands under pressure is quite different in the $k_\perp$ and k_z directions. The interchain interactions increase much faster than the intrachain ones which changes bands much more strongly in the $k_\perp$ direction. This is seen most clearly in the dramatic change near the conduction-band minimum on the $k_\perp$ axis of the more anisotropic Se where the effective mass decreases by 80% and the spin-orbit splitting increases about 1 order of magnitude when pressure is increased from 0 to 52 kbar.

ACKNOWLEDGMENTS

We wish to express our gratitude to Professor T. Stubb and Professor M. A. Ranta for their support and to the Computer Center of Helsinki University of Technology for amicable cooperation. The work of one of the authors (J.v.B.) was supported by the Academy of Finland. We wish to thank the Swedish Academy of Technical Sciences in Finland for financial support in connection with the publication.

APPENDIX: FUNDAMENTAL EQUATIONS AND COMPUTATIONAL ASPECTS

The equations to be presented in this appendix are fully general. The elements of the matrix of the perturbation operator in Eq. (1) is formed between the spin orbitals $\psi^n_{\vec{k}}\chi_{m_s}$ where $\psi^n_{\vec{k}}$ is the nonrelativistic Bloch eigenfunction (n is the band index and $\vec{k}$ the reduced wave vector) and χ_{m_s} the eigenfunction of $\vec{\sigma}^2, \sigma_z$ with eigenvalues $3, m_s$ ($m_s = \pm 1$). Because $\psi^n_{\vec{k}}$ are given as a linear combination of the orthogonalized plane waves $X_{\vec{k}_i}$ ($\vec{k}_i = \vec{k} + \vec{G}_i$ where $\vec{G}_i$ is a reciprocal-lattice vector) we need, in fact, matrix elements between the functions $X_{\vec{k}_i}\chi_{m_s}$. A lengthy calculation gives the following result:

$$
\begin{aligned}
&\left\langle X_{\vec{k}_i}\chi_{m_s}\left|-i\frac{\alpha^2}{4}\vec{\sigma}\cdot(\nabla V)\times\nabla X_{\vec{k}_j}\chi_{m_s'}\right.\right\rangle \\
&\quad = i\frac{\alpha^2}{4}V(\vec{G}_j-\vec{G}_i)\vec{\sigma}_{m_s m_s'}\cdot\vec{k}_i\times\vec{k}_j \\
&\qquad + \frac{4\pi^2\alpha^2}{\Omega_0}\sum_q e^{i(\vec{G}_j-\vec{G}_i)\cdot\vec{\tau}_q}\sum_{l=1}^{l_{\max}^q}[\;]_{m_s m_s'}\sum_{n=l+1}^{n_{\max}^q}\Bigg[-b_{nlk_j}^q\int_0^\infty j_l(k_i r)\frac{dV_s^q(r)}{dr}R_{nl}^q(r)r\,dr \\
&\qquad\qquad -b_{nlk_i}^q\int_0^\infty j_l(k_j r)\frac{dV_s^q(r)}{dr}R_{nl}^q(r)r\,dr \\
&\qquad\qquad +b_{nlk_i}^q\sum_{n'=l+1}^{n_{\max}^q}b_{n'lk_j}^q\int_0^\infty R_{nl}^q(r)\frac{dV_s^q(r)}{dr}R_{n'l}^q(r)r\,dr\Bigg]\,, \qquad \text{(A1)}
\end{aligned}
$$

$$
\begin{aligned}
&\left\langle X_{\vec{k}_i}\left|\frac{\alpha^2}{8}(\nabla^2 V)X_{\vec{k}_j}\right.\right\rangle = \\
&\quad -\frac{\alpha^2}{8}(\vec{G}_j-\vec{G}_i)^2 V(\vec{G}_j-\vec{G}_i) \\
&\quad +\frac{\pi\alpha^2}{2\Omega_0}\sum_q e^{i(\vec{G}_j-\vec{G}_i)\cdot\vec{\tau}_q}\sum_{l=0}^{l_{\max}^q}P_l(\cos\beta_{\vec{k}_i\vec{k}_j})(2l+1) \\
&\qquad \times\sum_{n=l+1}^{n_{\max}^q}\Bigg[-b_{nlk_j}^q\int_0^\infty j_l(k_i r)\left[\frac{2}{r}\frac{dV_s^q(r)}{dr}+\frac{d^2V_s^q(r)}{dr^2}\right]R_{nl}^q(r)r^2\,dr \\
&\qquad\qquad -b_{nlk_i}^q\int_0^\infty j_l(k_j r)\left[\frac{2}{r}\frac{dV_s^q(r)}{dr}+\frac{d^2V_s^q(r)}{dr^2}\right]R_{nl}^q(r)r^2\,dr \\
&\qquad\qquad +b_{nlk_i}^q\sum_{n'=l+1}^{n_{\max}^q}b_{n'lk_j}^q\int_0^\infty R_{nl}^q(r)\left[\frac{2}{r}\frac{dV_s^q(r)}{dr}+\frac{d^2V_s^q(r)}{dr^2}\right]R_{n'l}^q(r)r^2\,dr\Bigg] \\
&\quad +\frac{\pi\alpha^2}{2\Omega_0}\sum_q e^{i(\vec{G}_j-\vec{G}_i)\cdot\vec{\tau}_q}Z^q\left[1-\sum_{n=1}^{n_{\max}^q}R_{n0}^q(0)b_{n0k_j}^q\right]\left[1-\sum_{n=1}^{n_{\max}^q}R_{n0}^q(0)b_{n0k_i}^q\right], \qquad \text{(A2)}
\end{aligned}
$$

and

$$
\begin{aligned}
&\left\langle X_{\vec{k}_i}\left|-\frac{\alpha^2}{8}\nabla^4 X_{\vec{k}_j}\right.\right\rangle \\
&\quad = -\frac{\alpha^2}{8}k_j^4\delta_{\vec{k}_i\vec{k}_j}+\frac{\pi\alpha^2}{2\Omega_0}\sum_q e^{i(\vec{G}_j-\vec{G}_i)\cdot\vec{\tau}_q}\sum_{l=0}^{l_{\max}^q}P_l(\cos\beta_{\vec{k}_i\vec{k}_j})(2l+1) \\
&\qquad \times\sum_{n=l+1}^{n_{\max}^q}\Bigg[(k_i^4+k_j^4)b_{nlk_i}^q b_{nlk_j}^q \\
&\qquad\qquad -4b_{nlk_i}^q\sum_{n'=l+1}^{n_{\max}^q}b_{n'lk_j}^q\int_0^\infty[E_{nl}^q-V_s^q(r)]R_{nl}^q(r) \\
&\qquad\qquad\qquad \times r[E_{n'l}^q-V_s^q(r)]R_{n'l}^q(r)r\,dr\Bigg]\,. \qquad \text{(A3)}
\end{aligned}
$$

In Eqs. (A1)−(A3) $V(\vec{G}_j-\vec{G}_i)$ is a Fourier component of $V(\vec{r})$:

$$V(\vec{G})=\frac{1}{\Omega_0}\int_{\Omega_0} V(\vec{r})e^{i\vec{G}\cdot\vec{r}}d^3r \ , \tag{A4}$$

$$\vec{\sigma}_{11}=\langle \chi_1 \,|\, \vec{\sigma}\chi_1\rangle=-\vec{\sigma}_{-1-1}=\vec{u}_z \ , \tag{A5}$$

$$\vec{\sigma}_{1-1}=\vec{\sigma}^{*}_{-11}=\vec{u}_x-i\vec{u}_y \ , \tag{A6}$$

where $\vec{u}_x$, $\vec{u}_y$, and $\vec{u}_z$ are the Cartesian unit vectors, Ω_0 is the volume of the primitive unit cell, q labels the atoms in the primitive unit cell, $\vec{\tau}_a$ is the position vector of the atom q,

$$\begin{aligned}[\ ]_{11}&=-[\ ]_{-1-1}\\ &=\sum_{m=-l}^{l} Y^l_m(\theta_{\vec{k}_j},\varphi_{\vec{k}_j})^{*}Y^l_m(\theta_{\vec{k}_i},\varphi_{\vec{k}_i})m \ ,\end{aligned} \tag{A7}$$

$$\begin{aligned}[\ ]_{1-1}=\sum_{m=-l}^{l-1} & Y^l_{m+1}(\theta_{\vec{k}_j},\varphi_{\vec{k}_j})^{*}Y^l_m(\theta_{\vec{k}_i},\varphi_{\vec{k}_i})\\ &\times[l(l+1)-m(m+1)]^{1/2} \ ,\end{aligned} \tag{A8}$$

$$\begin{aligned}[\ ]_{-11}=\sum_{m=-l}^{l-1} & Y^l_m(\theta_{\vec{k}_j},\varphi_{\vec{k}_j})^{*}Y^l_{m+1}(\theta_{\vec{k}_i},\varphi_{\vec{k}_i})\\ &\times[l(l+1)-m(m+1)]^{1/2} \ ,\end{aligned} \tag{A9}$$

where Y^l_m are the spherical harmonics, b^q_{nlk} is the radial orthogonalization coefficient

$$b^q_{nlk}=\int_0^{\infty} R^q_{nl}(r)j_l(kr)r^2dr \ , \tag{A10}$$

where $R^q_{nl}(r)$ is the radial part of the core function of atom q and j_l the spherical Bessel function, V^q_s is the crystal potential spherically symmetrized around $\vec{\tau}_q$, P_l is the Legendre polynomial, and $\beta_{\vec{k}_i\vec{k}_j}$ the angle between $\vec{k}_i$ and $\vec{k}_j$, Z^q is the charge of the nucleus of atom q, and E^q_{nl} is the eigenenergy associated with R^q_{nl}.

The first term in Eq. (A1) is the plane-wave−plane-wave part, the first and second terms in the large parentheses correspond to the plane-wave-core parts and the third term in the large parentheses to the core-core part. In deriving the second term in Eq. (A1), containing all core parts, the spin-orbit operator was written into the well-known radial form:

$$\frac{\alpha^2}{4}\frac{1}{r}\frac{dV^q_s(r)}{dr}(\vec{j}^{\,2}-\vec{l}^{\,2}-\vec{s}^{\,2}) \ . \tag{A11}$$

It was moved to operate on the core functions with the use of the turnover rule, and the $Y^l_m\chi_{m_s}$ parts of the core functions were written for the operation in terms of the eigenfunctions of this operator by means of the Glebsch-Gordan coefficients.

In writing Eq. (A2) for the Darwin term it is important to take the singular part properly into account. ∇^2V around the nucleus q is

$$\nabla^2V^q_s(r)=\left[\frac{2}{r}\frac{dV^q_s(r)}{dr}+\frac{d^2V^q_s(r)}{dr^2}\right]_{r\neq 0}+4\pi Z^q\delta(\vec{r}) \ . \tag{A12}$$

The last term in Eq. (A2) is the singular part originating from the last term in Eq. (A12). In Eq. (A2) the positive singular part is much larger than the former (usually negative) part which reflects the difference between the actual $V(\vec{r})$ and $-Z^qr^{-1}$. In the former part the first term is the plane-wave−plane-wave part whereas the second term contains the core parts.

In deriving Eq. (A3) for the mass-velocity term the ∇^4 operator is moved to operate on the plane-wave part whenever possible (using the turnover rule) whereas in writing the core-core part [corresponding to the second term in the large parentheses of Eq. (A3)] the radial eigenvalue equation, written in the form

$$\nabla^2R^q_{nl}Y^l_m=-2[E^q_{nl}-V^q_s(r)]R^q_{nl}Y^l_m \ . \tag{A13}$$

and the turnover rule for ∇^2 are used.

Because the Darwin and mass-velocity operators have at least the same symmetry as the effective nonrelativistic crystal potential, only the diagonal matrix elements need to be calculated. At the VB maximum at point H the nonrelativistic eigenvalue is double degenerate (single group representation H_3). This leads to a 4×4 matrix for the spin-orbit operator. Because this degeneracy is reflected also to the neighborhood of point H the two uppermost nonrelativistic valence bands are treated together analogously to point H. Elsewhere (VB maximum at M, CB minimum at H) the nondegenerate nonrelativistic eigenvalue leads to a 2×2 matrix.

The symmetry orientated program system used in Ref. 46 could not be generalized to apply to general $\vec{k}$ points and compound crystals with any reasonable effort because of its very complicated structure. Also in these programs the Darwin correction was treated erroneously. Therefore, a new efficient (almost five times faster) single program was constructed for the present calculations. This program was tested as follows. The nondiagonal matrix elements of the Darwin and mass-velocity matrices, which should be zero, were about one tenth of the diagonal elements. The Hermiticity of all the three perturbation matrices was numerically perfectly valid. The matrix elements of the three perturbation matrices were tested against earlier results in some special cases and an agreement with at least four significant digits was obtained.

---

[1] M. Kastner and R. R. Forberg, Phys. Rev. Lett. 36, 740 (1976).

[2] F. Nizzoli, in *The Physics of Selenium and Tellurium,* edited by E. Gerlach and P. Grosse (Springer, Berlin, 1979), Vol. 13, p. 31.

[3] H. Wendel, R. M. Martin, and D. J. Chadi, Phys. Rev. Lett. 38, 656 (1977).

[4] J. D. Joannopoulos, T. Starkloff, and M. Kastner, Phys. Rev. Lett. 38, 660 (1977).

[5] A. R. Moodenbaugh, C. T. Wu, and R. Viswanathan, Solid State Commun. 13, 1413 (1973).

[6] R. Keller, W. B. Holzapfel, and H. Schulz, Phys. Rev. B 16, 4404 (1977).

[7] G. Doerre and J. D. Joannopoulos, Phys. Rev. Lett. 43, 1040 (1979).

[8] T. Starkloff and J. D. Joannopoulos, J. Chem. Phys. 68, 579 (1978).

[9] H. Isomäki and J. von Boehm, Solid State Commun. 34, 709 (1980).

[10] J. von Boehm and H. Isomäki, J. Phys. C 13, 4953 (1980).

[11] H. Isomäki, J. von Boehm, P. Krusius, and T. Stubb, Phys. Rev. B 22, 2945 (1980).

[12] F. P. Bundy and K. J. Dunn, Phys. Rev. Lett. 44, 1623 (1980).

[13] F. P. Bundy and K. J. Dunn, Phys. Rev. B 22, 3157 (1980).

[14] M. Lutz, in *The Physics of Selenium and Tellurium,* edited by E. Gerlach and P. Grosse (Springer, Berlin, 1979), Vol. 13, p. 86 and references therein.

[15] For a review see the paper by Yu. V. Kosichkin, in *The Physics of Selenium and Tellurium,* edited by E. Gerlach and P. Grosse (Springer, Berlin, 1979), Vol. 13, p. 96.

[16] V. B. Anzin, M. S. Bresler, I. I. Farbstein, E. S. Itskevich, Yu. V. Kosichkin, V. A. Sukhoparov, A. S. Telepnev, and V. G. Veselago, Phys. Status Solidi B 48, 531 (1971).

[17] A. Koma, T. Tani, and S. Tanaka, Phys. Status Solidi B 66, 669 (1974).

[18] V. B. Anzin, M. I. Eremets, Yu. V. Kosichkin, A. I. Nadezhdinskii, and A. M. Shirokov, Phys. Status Solidi A 42, 385 (1977).

[19] M. V. Glushkov, M. I. Eremets, Yu. V. Kosichkin, A. N. Tolmachev, and A. M. Shirokov, Fiz. Tverd. Tela (Leningrad) 21, 499 (1979) [Sov. Phys.—Solid State 21, 295 (1979)].

[20] B. Moreth, Phys. Rev. Lett. 42, 264 (1979).

[21] H. L. Suchan, S. Wiederhorn, and H. G. Drickamer, J. Chem. Phys. 31, 355 (1959).

[22] T. Starkloff and J. D. Joannopoulos, Phys. Rev. B 19, 1077 (1979).

[23] J. von Boehm and H. Isomäki, J. Phys. Soc. Jpn. 49, Suppl. A 121 (1980).

[24] J. von Boehm and H. Isomäki, Solid State Commun. (in press).

[25] P. Unger and P. Cherin, in *The Physics of Se and Te,* edited by W. C. Cooper (Pergamon, Oxford, 1969), p. 223. (Constants are slightly corrected to correspond to $T = 0$ K.)

[26] J. C. Jamieson and D. B. McWhan, J. Chem. Phys. 43, 1149 (1965).

[27] R. Keller, W. B. Holzapfel, and H. Schulz, in Refs. 8 and 22.

[28] D. R. McCann, L. Cartz, R. E. Schmunk, and Y. D. Harker, J. Appl. Phys. 43, 1432 (1972).

[29] D. R. McCann and L. Cartz, J. Appl. Phys. 43, 4473 (1972).

[30] J. C. Slater, Phys. Rev. 81, 385 (1951).

[31] L. Liu, Phys. Rev. 126, 1317 (1962).

[32] P. Soven, Phys. Rev. 137, A1706 (1965).

[33] F. H. Pollak, M. Cardona, C. W. Higginbotham, F. Herman, and J. P. Van Dyke, Phys. Rev. B 2, 352 (1970).

[34] G. G. Wepfer, T. C. Collins, and R. N. Euwema, Phys. Rev. B 4, 1296 (1971).

[35] Y. Couder, Phys. Rev. Lett. 22, 890 (1969).

[36] O. Betbeder-Matibet and M. Hulin, Phys. Status Solid 36, 573 (1969).

[37] T. Doi, K. Nakao, and H. Kamimura, J. Phys. Soc. Jpn. 28, 822 (1970).

[38] K. Nakao, T. Doi, and H. Kamimura, J. Phys. Soc. Jpn. 30, 1400 (1971).

[39] N. Miura, R. Yoshizaki, and S. Tanaka, Solid State Commun. 7, 1195 (1969).

[40] R. Yoshizaki and S. Tanaka, J. Phys. Soc. Jpn. 30, 1389 (1971).

[41] P. L. Radoff and R. N. Dexter, Phys. Status Solidi 35, 261 (1969).

[42] B. Kramer and P. Thomas, Phys. Status Solidi 26, 151 (1968).

[43] E. Bangert, D. Fischer, and P. Grosse, Phys. Status Solidi B 59, 419 (1973).

[44] H. Stolze, M. Lutz, and P. Grosse, Phys. Status Solidi B 82, 457 (1977).

[45] H. Shinno, R. Yoshizaki, S. Tanaka, T. Doi, and H. Kamimura, J. Phys. Soc. Jpn. 35, 525 (1973).

[46] P. Krusius, J. von Boehm, and T. Stubb, Phys. Status Solidi B 67, 551 (1975).